Tunable crystal structure of Cu_2SnS_3 thin films deposited by spray pyrolysis and its impact on the chemistry and electronic structure

R. Garza-Hernández [1], H.J. Edwards [2], J.T. Gibbon [2], M.R. Alfaro Cruz [3], V.R. Dhanak [2*], F.S. Aguirre-Tostado [1*].

[1] Centro de Investigación en Materiales Avanzados S. C. (Unidad Monterrey), Av. Alianza Norte 202, Autopista Monterrey-Aeropuerto km 10, PIIT, Apodaca, Nuevo León, C.P. 66628, México.

[2] Department of Physics, Stephenson Institute for Renewable Energy, University of Liverpool, L69 7ZF Liverpool U.K.

[3] CONACYT–Universidad Autónoma de Nuevo León, Facultad de Ingeniería Civil, Departamento de Ecomateriales y Energía, Av. Universidad S/N Ciudad Universitaria, San Nicolás de los Garza, Nuevo León, C.P. 66455, México.

E-mail address: servando.aguirre@cimav.edu.mx, V.R.Dhanak@liverpool.ac.uk

*** Corresponding author**

KEYWORDS: Cu_2SnS_3, spray pyrolysis, photoelectron spectroscopy, thin-film, band alignment, inverse photoelectron spectroscopy, electronic structure.

Abstract

Cu_2SnS_3 (CTS) thin films were grown by spray pyrolysis method on Mo substrates. Two different synthetic routes: stoichiometric and non-stoichiometric in aprotic media are proposed. The use of dimethyl sulfoxide (DMSO) as a solvent improved the solubility of metal chlorides at room temperature, which was crucial to avoid the metal-hydroxylation. In this sense, a reaction mechanism for forming CTS films considering an aprotic media ~~is~~ proposed. Both routes and different sulfurization temperatures (350, 400, 500, 560, and 600 °C) allowed the presence of different crystalline structures of Cu2SnS3, corroborated by Raman Spectroscopy and X-ray diffraction measurements. For the non-stoichiometric composition (Cu/Sn = 1.76) and a temperature annealing interval of 350-600 °C, the films were composed of a monoclinic-Cu_2SnS_3 phase. For the stoichiometric composition (Cu/Sn = 2), the films constituted a tetragonal-Cu_2SnS_3 phase as long as the temperature was in the range of 300 and 400 °C. When increasing the temperature up to 500 °C, the Cu content increased, and the orthorhombic-Cu_3SnS_4 phase was formed. X-ray photoelectron spectroscopy (XPS) was used to determine the surface composition, chemical states, valence band, and core levels of the films. These measurements confirm that the samples are constituted by Sn^{4+} and Cu^{+}, which were corroborated by the Auger parameters. The proximity of the valence band maximum (VBM) to the Fermi level confirms these compounds are p-type by nature. Electronic structures of the films surface were obtained by XPS combined with inverse photoemission spectroscopy (IPES). The tetragonal, orthorhombic, and monoclinic films exhibit an electronic bandgap of 1.33 eV, 1.25 eV, and 1.15 eV, respectively, at the surface. This leads to a small cliff in the conduction band alignment at the CdS/CTS interface.

1. Introduction

Several solar technologies have been researched to achieve cost-effectiveness, reliability, and high efficiency with success. Thin films solar cells can satisfy minimum material usage and high energy conversion efficiency. CdTe and $CuInGaSe_2$ are the most chalcogenide semiconductors used as an alternative to silicon in thin film solar cells [1-3]. Nevertheless, these materials contain elements that are toxic, scarce, and costly. An ecofriendly alternative to replace these chalcogenides is the use of Cu_2ZnSnS_4, which contains elements that are abundant and less toxic than the $CuInGaSe_2$ and CdTe [4]. Unfortunately, the Cu_2ZnSnS_4 films are susceptible to the formation of secondary phases and surface contamination since it is difficult to have full control over the quaternary system growth conditions. In this sense, the control of composition in a ternary system is more feasible due to its fewer elements than the quaternary system. That is why some ternary compounds have been investigated as candidates for photovoltaic absorbers, including Cu_2SnS_3, Cu_3SnS_4, Cu_4SnS_4, $Cu_2Sn_3S_7$, and $Cu_5Sn_2S_7$ [5-7]. Mainly, Cu_2SnS_3 material exhibits a p-type semiconductor nature with a high optical absorption coefficient ($\alpha>10^4$ cm^{-1}) and a direct band gap of about 0.8-1.7 eV [8, 9]. Additionally, thin film solar cells based on Cu_2SnS_3 have reached a conversion efficiency of 4.29% [10].

The physicochemical properties of Cu_2SnS_3 thin films depend on the crystalline structure, synthesis method, and the annealing temperature. Cu_2SnS_3 has different crystalline structures such as cubic, monoclinic, tetragonal and triclinic, which have been reported for this compound in a range of 25-780°C [11-14]. These phases have been synthesized by various deposition techniques such as sputtering [15, 16], electron beam evaporation [17], pulsed laser deposition [18], chemical vapor deposition [19], co-evaporation [20], chemical bath deposition [11, 21, 22], spray pyrolysis [23-28], etc. Particularly, solution-based non-vacuum techniques, such as spray pyrolysis, represent ~~a~~ commercial significance for their low process cost. Spray pyrolysis is an inexpensive, versatile, and straightforward technique that controls chemical composition. Many works related to the synthesis and characterization of Cu_2SnS_3 thin films deposited by spray pyrolysis have been published. Most of the publications are focused on the variation of some parameters such as

precursor concentration, type of solvent, droplet size, and the distance between the nozzle to the substrate, substrate temperature, solution flow rate/spray rate and atmosphere annealing [23-28].

To get stoichiometric, single-phase, and homogeneous Cu_2SnS_3 thin films by spray pyrolysis it is necessary to consider three principal factors: the solvent, the optimum molar concentrations, and the atmosphere of thermal annealing. These factors play an important role in preventing chemical oxidation and the formation of secondary phases. About the first factor, deionized water and methanol are the most used solvents in synthesizing Cu_2SnS_3 by this method. Although copper chloride (II) salt is soluble in water at 20 °C, tin chloride (II) salt is soluble in water only at 0°C, which promotes the hydrolysis at room temperature [29]. The tin chloride behavior can cause in-situ oxidation, forming highly stable oxides difficult to remove after the thermal annealing. Moreover, the use of low boiling point alcohols (< 100 °C) as solvents is not recommended, due to the instantaneous and uncontrolled evaporation carried out at this temperature, causing large aggregates and pores in the films. For that, dimethyl sulfoxide (DMSO) is an aprotic solvent to avoid these problems. The copper and tin chloride salts are soluble in it at room temperature, and its high boiling point (189 °C) allows the slow and controlled evaporation for getting of a homogeneous film. About, molar concentration, it is important to consider that the precursor solution is not directly related to the final concentration of the film due to its dependence of the solvent viscosity, the complexes formed in the aprotic media and the temperature of evaporation. Additionally, the atmosphere and the temperature of the thermal annealing are crucial to achieving a single phase thin film. The loss of sulfur (> 200 °C), which is well known in this kind of system, promotes the segregation of Cu_2S [5, 30]. Some authors suggest using a sulfur atmosphere to avoid the presence of secondary phases and favor the increment of crystal size.

In this sense, the recognition of secondary phases in polymorphic Cu_2SnS_3 thin films requires a detailed characterization. Moreover, experimental studies of the band structures of Cu_2SnS_3 can allow the determination of the electronic band positions and the band gap, which is relevant in the fabrication of a photovoltaic device. However, few authors, who studied the effect of annealing temperature on Cu_2SnS_3 thin films by spray pyrolysis, focused on a small number of

temperature values without enquiring about structural or chemical characterization. Furthermore, few experimental studies related to the determination of the electronic properties of Cu_2SnS_3 have been explored. Thus, in this paper, we present a thorough experimental study of the effect of composition, reaction and annealing temperature in conjunction with the electronic properties of the synthesized materials. A reaction mechanism for the formation of CTS using DMSO as a solvent is proposed.

2. Experimental Details

2.1 Thin film deposition

Cu_2SnS_3 thin films were deposited onto the molybdenum coated soda lime (Mo-SLG) glass substrates with dimensions of 10 mm x 10 mm x 3mm by spray pyrolysis method. In this work, two different approaches, stoichiometric and non-stoichiometric routes, are proposed. All chemicals used for the deposition process were analytical grade from Sigma Aldrich. The molar concentration for non-stoichiometric and stoichiometric precursor solutions were 0.103 M $CuCl_2$, 0.060 M $SnCl_2$, 0.288 M thiourea and 0.096 M $CuCl_2$, 0.048 M $SnCl_2$, 0.144 M thiourea, respectively. The precursors were dissolved in 25 mL of dimethyl sulfoxide (DMSO) and stirred for 10 minutes until getting a transparent solution. The precursor solution was pulsed-intermittently sprayed 10 times (stopping for 60 s between each spray) onto a heated substrate (300 °C) using an airbrush. The distance between the nozzles to the substrate was kept at 30 cm. After deposition, the films were annealed in a tubular quartz furnace. A rotary pump was used to evacuate the system. The films were then collected in a graphite box with 0.1 g of sulfur powder. The thin films were annealed at six different temperatures: 350, 400, 500, 560, and 600°C under the nitrogen atmosphere for 10 minutes. The pressure in the tube was kept at 300 Torr. A representative scheme of the experimental procedure is shown in **Figure 1**.

2.2 Characterization

The crystalline structure of the Cu_2SnS_3 thin films was studied using a Rigaku SmartLab diffractometer with CuKα radiation of a wavelength of 1.5406 Å. A grazing incidence mode

(Ω=1°) was used to perform the measurements. The scan 2θ range was from 10 to 90° with a step of 0.01° and speed time of 3.00°/min. Also, Raman spectra were collected with a 633 nm wavelength laser using a Renishaw via Reflex spectrometer with a microscope (Leica) focused via 20X objective (Leica). All the spectra are baseline corrected for clarity. The chemical composition was obtained by Energy dispersive X-ray microanalysis (EDX) with an Oxford INCA X-act EDX detector in a JEOL JSM 6610 scanning electron microscope. X-ray photoelectron spectroscopy (XPS) was used to determine the surface composition, chemical states, valence band, and core levels of the samples. The measurements were performed in a standard ultra-high vacuum (UHV) chamber with a base pressure below $2x10^{-8}$ Pa. The photoelectrons were generated with a monochromatic Al Kα SPECS XRC-1000 source radiation (1486.6 eV) operating at 250W in conjunction with PSP Vacuum Technology electron energy analyzer with a pass energy of 10 eV. The spectrometer was calibrated using the Ag 3d core levels from a sputtered silver foil with a full-width at half maximum of 0.6 eV, thus the resolution of the core levels are ± 0.1 eV. By fitting the fermi level from the foil, the resolution for the Fermi edge was determined to be 0.37 ± 0.06 eV. To determine the vacuum level, the secondary electron cutoff (SEC) measurement at low kinetic energies was carried out by applying -20V bias to the sample to separate the sample secondary electrons from the spectrometer. Corrections of the shift in the binding energy were made by fixing the energy of the C1s peak, from adventitious carbon in the films, at 284.8 eV. Inverse photoemission spectroscopy (IPES) was performed using a PSP Vacuum Technology BaO cathode dispensor electron source and an isochromat NaCl photon detector, both at an angle of 45^0 to the sample normal. The IPES spectrometer was calibrated using the known energy position of the lowest unoccupied orbital of multilayer C_{60} film deposited in-situ in the spectrometer, as well as using the fermi level of sputtered silver foil. The IPES resolution was determined to be 1.00 ± 0.17 eV. The photoemission core-level fitting procedure was an iterative process whereby all peaks were fitted using AAnalyzer® peak fitting software. Optical transmittance and specular reflectance spectra were measured with a SolidSpec-3700i UV-VIS-NIR spectrophotometer from Shimadzu, in the spectral range from 1100 to 300 nm.

3. Results and Discussion

3.1 Reaction Mechanism

Figure 1 (top) shows the mechanism proposed in this work considering all the synthesis precursors. Copper and tin chloride salts were dissolved in DMSO. The copper and tin ions coordinate with the DMSO molecules forming a metal complex (A). The coordination numbers of the copper and tin atoms (4, 5, and 6) depend on the ligand and the oxidation number. This factor influences the production of different structures as tetrahedral, trigonal bipyramid, or octahedral [31, 32]. The presence of different bonds C=S (thiourea) or C-SH (isothiourea) is due to the tautomerization of thiourea. This process is carried out as a reversible intramolecular proton migration. Once the metal ions are solvated, this group can displace the DMSO molecules from the structure, depending on the interactive force between the ligand and the metal. Then, the metal ions can interact with the sulfur atom from thiourea (B) or NH=C from isothiourea (C). When the solution is completely transparent, it spills on a hot surface. At this time, the solvent evaporates, forming the CTS compound (D). It is possible that during the heating step, different compounds such as NH_3, CO_2, H_2S, NHCS, and HN-C-NH, which are highly volatile, are evaporated.

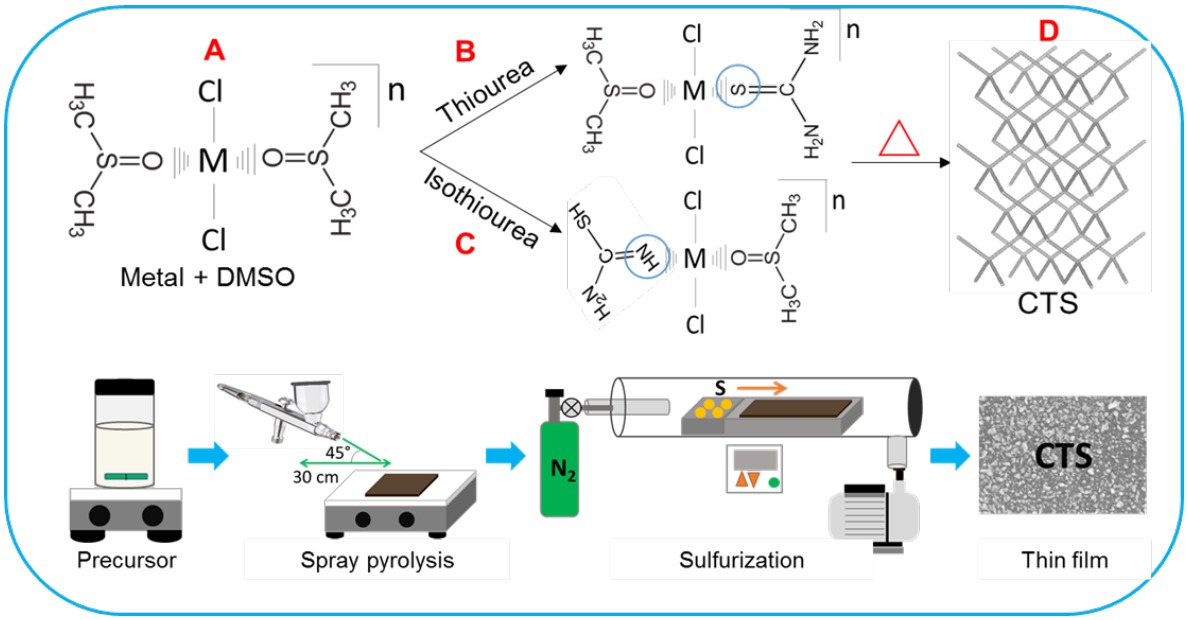

Figure 1. Top) Reaction mechanism for the formation of CTS using DMSO as a solvent considering the tautomerization of thiourea. Down) Schematic representation of the experimental procedure to obtain CTS thin films.

3.2 Energy dispersive X-ray (EDX)

The elemental compositions for the CTS thin films obtained by the two different approaches are shown in Table 1. The tendency observed for each element through the annealing temperature is kept for the two methods. These results indicate that by increasing the annealing temperature, the amount of tin diminishes. A. Weber et al. conclude that the Sn loss occurs above 460 °C due to tin sulfide evaporation on account of its high vapor pressure [33]. Besides, the sulfurization process allows compensating for the loss of sulfur during the thermal annealing, keeping the atomic concentration around 50%. The stoichiometric approach results in Cu-rich thin films, promoting the formation of phases such as CuS, Cu_2S, Cu_3SnS_4, and Cu_4SnS_4.

Table 1. EDX Chemical compositions of CTS thin films obtained by non- stoichiometric and stoichiometric approaches annealed at different temperatures.

	Non-stoichiometric approach					Stoichiometric approach				
T (°C)	Cu (%)	Sn (%)	S (%)	S/Cu+Sn	Cu/Sn	Cu (%)	Sn (%)	S (%)	S/Cu+Sn	Cu/Sn
350	29	19	52	1.08	1.53	34	14	52	1.08	2.43
400	28	19	53	1.13	1.47	35	16	49	0.96	2.19
500	31	16	53	1.13	1.94	36	13	51	1.04	2.77
560	31	17	52	1.08	1.82	37	13	50	1.00	2.85
600	32	16	52	1.08	2.00	38	12	50	1.00	3.17

3.3 Raman spectroscopy

Raman spectroscopy was performed to determine the CTS phases in the samples. The principal vibration modes for the CTS reported are: 303 cm^{-1} and 355 cm^{-1} for cubic, 296 cm^{-1} and 336 cm^{-1} for tetragonal and 290 cm^{-1} and 352 cm^{-1} for monoclinic phases [34-40]. **Figure 2** shows the Raman spectra for the thin films synthesized by both approaches, and several temperature values. The crystallinity improves as the temperature increase in the non-stoichiometric approach. The

peaks located in 292 cm^{-1} and 353 cm^{-1} are attributed to the monoclinic Cu_2SnS_3 phase. The area ratio of these peaks decreased when the annealing temperature increases, which is consistent with that Baranowski *et al.* observed when the amount of copper in the samples is high [5, 34]. This behavior is consistent with our previous EDX results.

In the case of the stoichiometric approach on the other hand, two different types of spectra can be obtained depending on the temperature. The Raman spectra for the annealed films at 350 °C and 400 °C show the main vibrational mode at 331 cm^{-1} for the tetragonal Cu_2SnS_3 structure. The crystallinity is improved when a temperature of 400 °C is reached. However, above this temperature, there is a preferred vibrational mode in 314 cm^{-1}, previously reported for the orthorhombic Cu_3SnS_4 phase [12, 39]. Therefore, in the stoichiometric approach, copper concentration and the annealing temperature induce a phase transformation. If the chemical composition is analyzed, three central regions can be specified: in the range of $1.47 \leq [Cu/Sn] \leq 2.00$, the main phase is monoclinic Cu_2SnS_3. In contrast, in the range of $2.19 \leq [Cu/Sn] \leq 2.43$, the predominant phase is tetragonal Cu_2SnS_3, and in the range at the higher copper concentration ($2.77 \leq [Cu/Sn] \leq 3.17$) the principal phase is orthorhombic Cu_3SnS_4.

The films annealed at 400 and 500 °C by the stoichiometric approach and the film annealed at 600 °C by the non-stoichiometric approach were chosen for their subsequent characterization. Any peak related to Cu_2S at 472 cm^{-1} was not perceived [41].

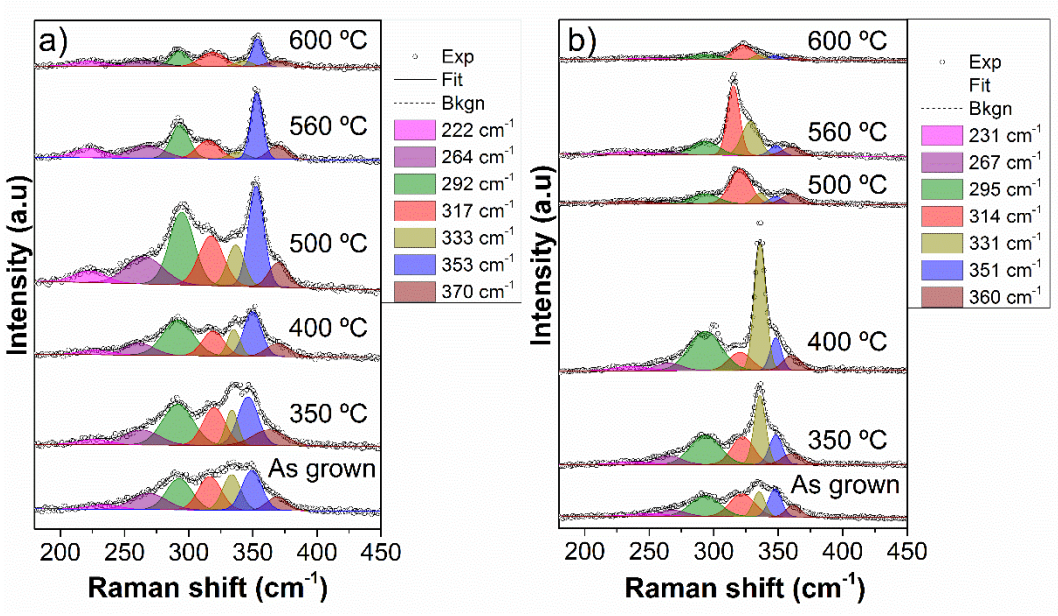

Figure 2. Raman spectra for Cu_2SnS_3 thin films obtained by the (a) non-stoichiometric and (b) stoichiometric approaches.

3.4 X-ray diffraction

X-ray diffraction was used to corroborate the phases found by Raman spectroscopy. **Figure 3** shows the diffraction patterns for the three samples chosen for further characterization. Comparison of the experimental diffractograms was made considering the JCPDS patterns of the three structures: monoclinic-Cu_2SnS_3 (04-010-5719), tetragonal-Cu_2SnS_3 (04-009-7947) and orthorhombic Cu_3SnS_4. Additionally, cubic Mo (00-042-1120) and cubic Cu_2S patterns were added to this comparison for complete discrimination. The two film patterns obtained from the stoichiometric approach at temperatures 400 °C and 500 °C differ. Four main peaks were observed for tetragonal Cu_2SnS_3 sample at 28.6°, 33.17°, 47.6° and 56.5° related to (112), (200), (220) and (312), respectively.

It is possible to see that most of the peaks from the samples are very similar and allow the conclusion that the patterns with tetragonal and monoclinic structure belonging to CTS. However, for the Cu_3SnS_4 phase, some peaks in the range 28-30 ° region are unique to this structure, so that this phase can be discerned among the others. The peaks located at 40° and 77 ° are attributed to

the substrate (Mo). The lattice parameters for the CTS samples are shown in Figure 3b, which agrees with that reported in the literature [12, 39].

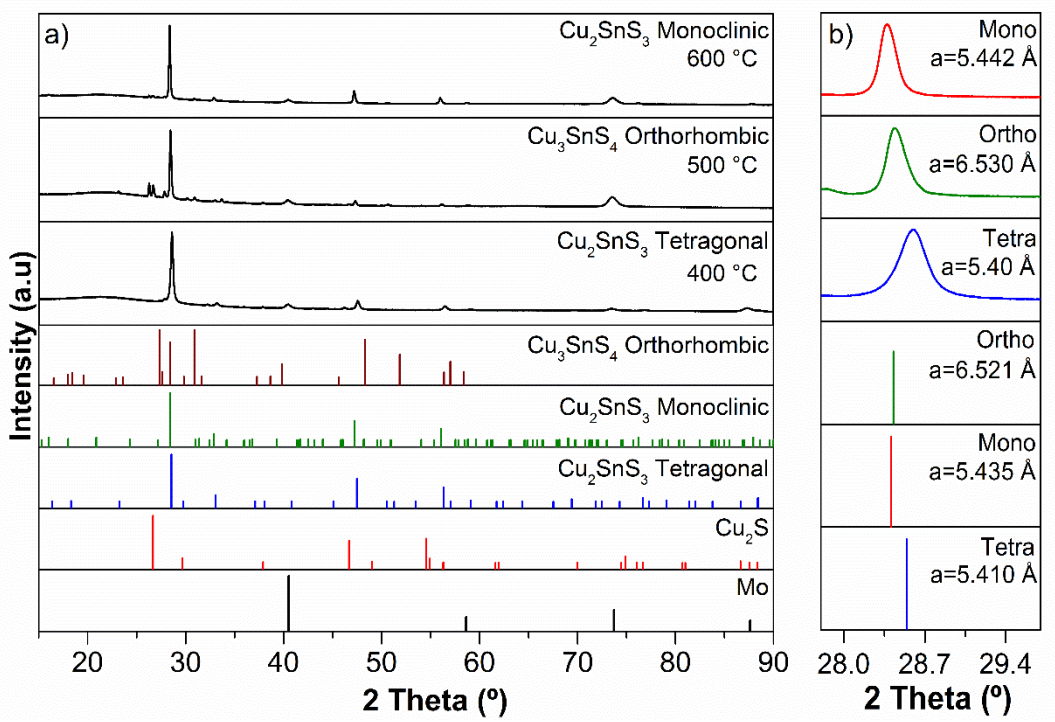

Figure 3. a) XRD patterns of tetragonal-Cu_2SnS_3, orthorhombic-Cu_3SnS_4, and monoclinic-Cu_2SnS_3 samples. b) Lattice parameter considering the most intense reflection peak.

3.5 UV-VIS spectroscopy

The optical absorption coefficients (α) of the films at different wavelengths were estimated from the transmittance (T) and reflectance (R) measurements using the following equation:

$$\alpha = \frac{1}{t}\ln\frac{(1-R)^2}{T} \quad (1)$$

where t is the thickness of the thin film, and λ is the wavelength of the photon. The optical bandgap (E_g) was calculated using the Tauc model:

$$\alpha h\upsilon = A\,(h\upsilon - E_g)^m \quad (2)$$

where A is a constant and "m" depends on the nature of conversion, which is equivalent to ½ or 2 for direct and indirect transitions, respectively [42].

The estimation of bandgap energy was made by extrapolating the linear region in the plot $(\alpha h\nu)^2$ up to the intersection with hν axis (**Figure 4**). Many studies have shown different bandgap energies between 0.93-1.77 eV [12, 43]. Specifically, the tetragonal-Cu_2SnS_3 film shows the main bandgap of 1.28 eV. On the other hand, a few authors show evidence of two absorption edges in Cu_2SnS_3 at 0.92-0.93 eV and 0.99-1.02 eV [44-46]. Two bandgaps were found in orthorhombic-Cu_3SnS_4 and monoclinic-Cu_2SnS_3 films. The bandgaps found for orthorhombic-Cu_3SnS_4 were 1.07 eV and 1.25 eV, while for the monoclinic- Cu_2SnS_3 they were 0.88 eV and 0.96 eV. Zhait *et al.* reported different structures with Cu_4Cu_3Sn, Cu_2Sn_2, $CuSn_3$, and Sn_4 clusters in Cu_2SnS_3, for which the band gaps differ by only a small amount [47]. The variation in Cu/Sn order parameter could cause these fluctuations in the bandgaps on the order of 0.1 eV.

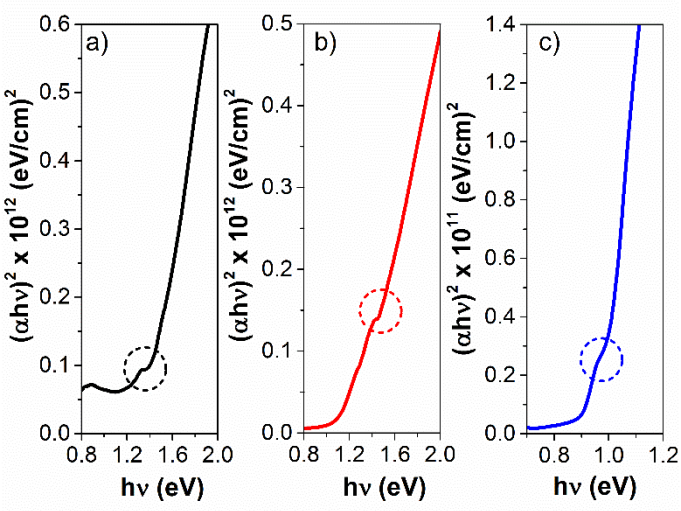

Figure 4. Bandgap energy estimation using $(\alpha h\nu)^2$ vs hν plots of the (a) tetragonal-Cu_2SnS_3 (400 °C), (b) orthorhombic-Cu_3SnS_4 (500 °C) and (c) monoclinic-Cu_2SnS_3 (600°C).

3.6 X-ray photoelectron spectroscopy (XPS) and Inverse photoemission spectroscopy (IPES)

High resolution spectra of the Cu 2*p*, Sn 3*d*, and S 2*p* core levels were fitted using a Shirley background. A comparison between the Cu 2*p* peaks of the three phases is shown in **Figure 5a**. The Cu 2*p* region is constituted by the Cu $2p_{3/2}$ and Cu $2p_{1/2}$ core levels. The oxidation state reported for copper in the tetragonal Cu_2SnS_3, orthorhombic Cu_3SnS_4, and monoclinic Cu_2SnS_3 structures are Cu (I). A high-intensity doublet peak for all samples was observed at 932.1 ± 0.1

eV with a spin-orbit splitting of 19.8 eV associated with Cu (I) [19, 48, 49]. The small peak at 933.2 ± 0.1 eV observed on tetragonal Cu_2SnS_3 sample is attributed to CuS [50, 51]. The absence of satellite peaks at 944 eV and 963 eV corroborates the lack of CuO and $Cu(OH)_2$ compounds in the samples [52, 53]. The corresponding comparison of Sn 3*d* features is shown in **Figure 5b**. A doublet peak located at 486.4 ± 0.1 eV with a spin-orbit splitting of 8.41 eV and an area ratio of 2:3 is associated with Sn (IV) [19, 48, 49]. Finally, the S 2*p* core level spectra show a doublet peak centered at 161.55 eV with a spin-orbit separation of 1.18 eV and an area ratio of 1:2, corresponding to $2p_{1/2}$ and $2p_{3/2}$ features, respectively. This binding energy is related to metal-sulfide bonds, where the S is in an oxidation state of -2 [48, 49]. A peak located at higher binding energy (162.4 eV) is observed on the tetragonal Cu_2SnS_3 sample, which can be associated with CuS compound [50, 51]. The Lorentzian and Gaussian width of each component was kept constant.

The Cu *2p*, Sn *3d*, and S *2p* line intensities, corrected for the appropriate atomic sensitivity factors (ASF), were used to determine the surface atomic composition of the CTS samples. The ASF values were obtained from the Scofield table. The atomic concentration percentages obtained by XPS for tetragonal Cu_2SnS_3, orthorhombic Cu_3SnS_4 and monoclinic Cu_2SnS_3 samples are shown in **Figure 5d**. The semi-quantitative analysis indicates that there are sulfur deficits in the three structures. The quantity of sulfur in the tetragonal Cu_2SnS_3 and orthorhombic Cu_3SnS_4 thin films is lower than the monoclinic Cu_2SnS_3 thin film. These results are directly related to the amount of copper in the samples. When the Cu content increases, the sulfur content diminishes, promoting the formation of Cu_2S compound. Also, the copper and tin diffusion to the surface is frequent in this system, so the concentration of these elements is higher than those obtained by EDX which is more bulk sensitive compared to XPS.

In addition to the photoelectron peak position, the shape and the position of Auger peaks can also help determine chemical states. Biesinger analyzed the shape of the peaks from different copper compounds and observing prominent differences between them, making it possible to discriminate between different comounds [54]. Based on this work, **Figure 5e** shows the Cu

$L_3M_{4,5}M_{4,5}$ peaks ~~position~~ centered at 569 eV and the two inflections observed at 566 eV and 573 eV, which are features of Cu (I) [55]. On the other hand, the position of the Sn $M_4N_{4,5}N_{4,5}$ and Sn $M_5N_{4,5}N_{4,5}$ peaks at 1052.1 eV and 1059.8 eV, respectively, are features of Sn (IV) [54 - 56].

The modified Auger parameters (α´) of Cu and Sn, which were calculated from the sum of the binding energy of Cu 2 $p_{3/2}$ or Sn 3 $d_{5/2}$ photoemission lines and the kinetic energy of the Cu $L_3M_{4,5}M_{4,5}$ or Sn $M_4N_{4,5}N_{4,5}$ Auger line, are shown in **Figure 5f**. The color shadow represents the ranges for Cu (I), Cu (II), Sn (0), Sn (II) and Sn (IV) compounds reported in the literature. Within the experimental uncertainty, the modified Auger parameters calculated for copper and tin for the three samples are within the range assigned for Cu (I) and Sn (IV) in the NIST database. Even when all the samples contain the same oxidation state (Cu^+ and Sn^{4+}), a charge compensation tendency between them is perceived.

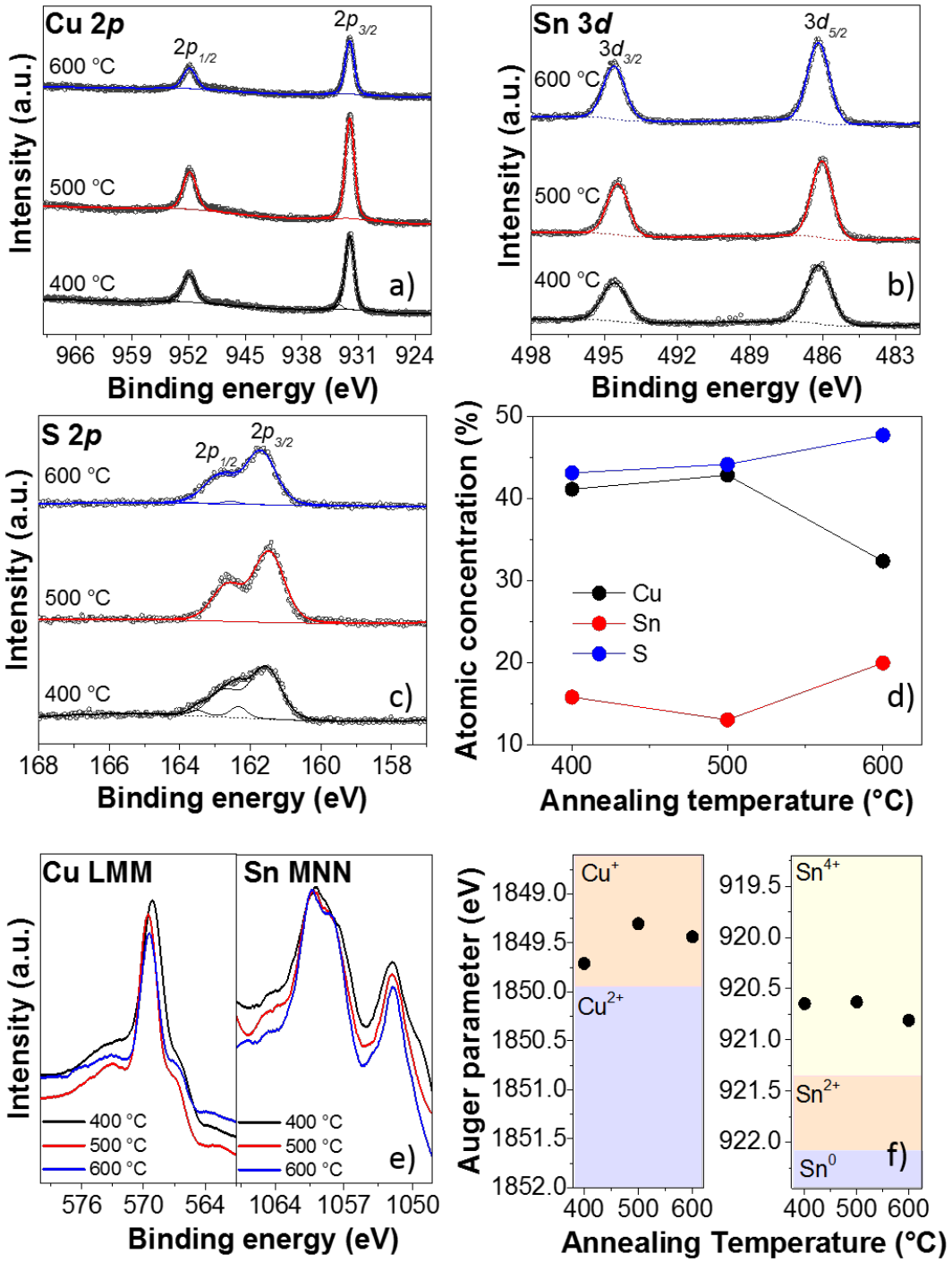

Figure 5. (a-c) XPS spectra for Cu 2*p*, Sn 3*d* and S 2*p* core levels, (d) surface atomic composition, (e) Cu LMM and Sn MNN peaks and (f) Auger parameters for tetragonal Cu_2SnS_3 (400 °C), orthorhombic Cu_3SnS_4 (500°C) and monoclinic Cu_2SnS_3 (600 °C) samples.

Band Alignment

From a device physics point of view, the most critical aspect of a semiconductor heterojunction interface is the energy-band diagram, which determines the charge transfer properties. It should be noted that most works related to the determination of these kinds of properties are obtained by electrical characterization. The solid lines in **Figure 6** indicate the linear extrapolation of the XPS and IPES spectra leading edges to determine the valence band maxima (VBM) and conduction band minimum (CBM), respectively. With relation to the vacuum level, the band positions allow the extraction of the values of electron affinity (EA), work function (WF), ionization potential (IP), and bandgap (Eg) [57]. These values are listed in **Table 2**.

Table 2. Band electronic parameters for tetragonal-Cu_2SnS_3 (400 °C), orthorhombic-Cu_3SnS_4 (500°C) and monoclinic-Cu_2SnS_3 (600 °C) samples.

Samples	VBM	CBM	E_g	E_{VAC}	IP	EA
400 °C	0.10	1.23	1.33	4.98	5.08	3.75
500 °C	0.12	1.13	1.25	5.38	5.50	4.25
600 °C	0.09	1.06	1.15	5.23	5.32	4.17

There are comparatively few studies of CTS in which electronic properties are obtained by XPS [51-53]. The measured Eg of 1.33 ± 0.18 eV for tetragonal Cu_2SnS_3, and the Eg of 1.15 ± 0.18 eV for monoclinic Cu_2SnS_3 are in agreement with previous studies [58-60]. The electronic Eg values determined by XPS are slightly higher (~0.15 eV) compared with those obtained by UV-Vis spectroscopy. On the other hand, the VBM and CBM reported for Cu_2SnS_3 are around 0.20 eV and 1.15 eV, respectively. In this work, the VBM values are found to be slightly lower than other studies. The proximity of the VBM to the Fermi level in all the samples confirms that these ternary compounds exhibit the expected p-type nature.

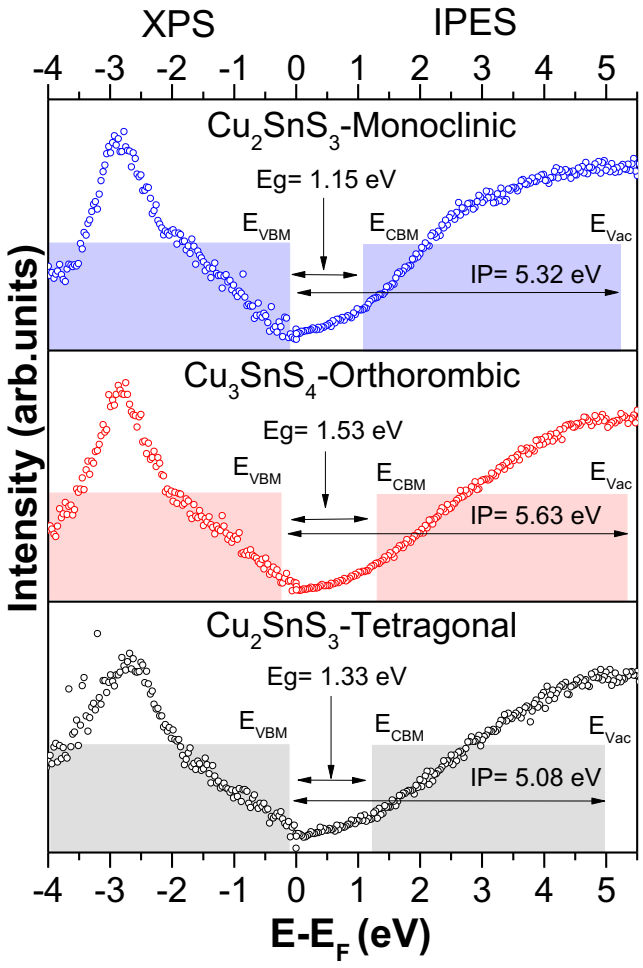

Figure 6. Band edge fitting and energy level determination for the three CTS samples.

The determination of the band alignment diagram helps to understand and to optimize the solar cell properties. Usually, CdS has been used as the buffer layer for CTS solar cells. **Figure 7** shows the three samples flat bands with the calculated IP and Eg from XPS/IPES measurements. CdS values were obtained from the literature. Because CTS samples were measured from the surface of thin films (~200 nm), any possible band bending was not considered.

A "cliff-like" band alignment occurs in the CdS/CTS interface, which can be recognized through the band gap reduction, promoting the recombination between electrons in the conduction band of the CdS and holes in the valence band of CTS. A small cliff in the conduction band alignment for tetragonal-Cu_2SnS_3 (400 °C), orthorhombic-Cu_3SnS_4 (500°C) and monoclinic-Cu_2SnS_3 (600 °C) samples of -0.43, -0.33 and -0.26 eV (± 0.19 eV) was observed with a significant valence band offset (hole barrier) of 1.50, 1.48 and 1.51 eV (± 0.08 eV), respectively.

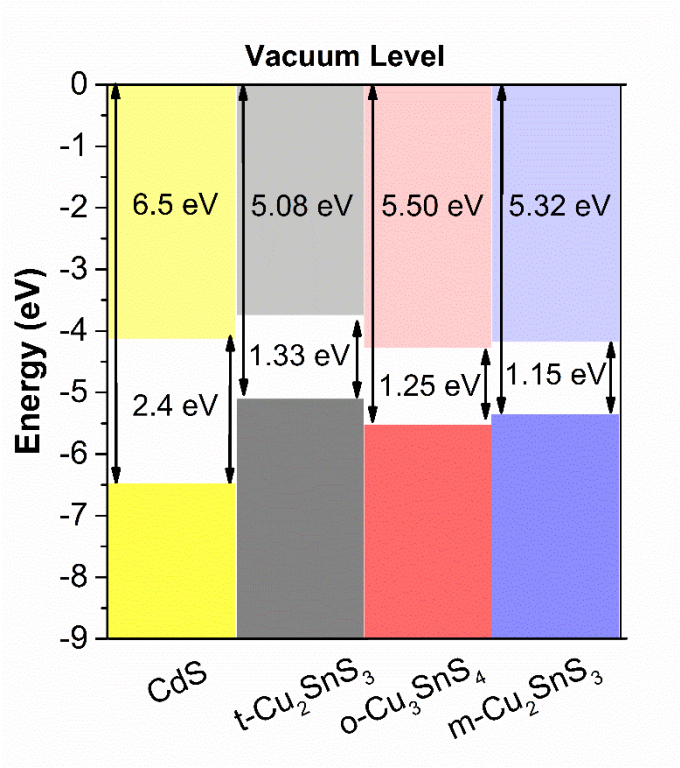

Figure 7. Vacuum-align band for tetragonal-Cu_2SnS_3 (400 °C), orthorhombic-Cu_3SnS_4 (500°C) and monoclinic-Cu_2SnS_3 (600 °C) samples. The most window layer (n-type) used in a solar cell is compare with the absorber layer (p-type).

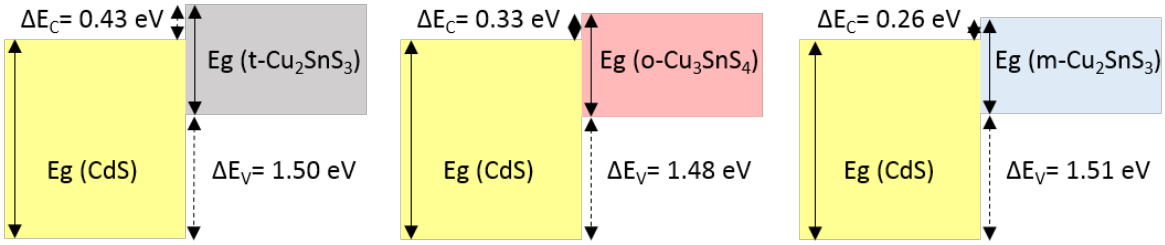

Figure 7.

4. Conclusions

Cu_2SnS_3 (CTS) thin films were deposited successfully using the spray pyrolysis method. Two different routes are proposed to improve the quality of the films. After deposition, the films were annealed at different temperatures. In the non- stoichiometric approach, the films showed the monoclinic Cu_2SnS_3 phase, while for the stoichiometric approach, the films annealed at 350 °C

and 400 °C showed the tetragonal phase of the Cu_2SnS_3. Above 400°C, the Cu_3SnS_4 films showed the orthorhombic phase. The presence of a secondary phase was corroborated by XPS measurements. The measurements show a small contribution from CuS in the tetragonal Cu_2SnS_3 film for the stoichiometric approach. The oxidation states were determined from the shape of the Auger peaks from which it was possible to corroborate that the oxidation states in all films were Cu^+ and Sn^{4+}. The band gap for each film was determined using the position of the valence band maxima (VBM) and conduction band minimum (CBM) from the XPS and IPES measurements. The obtained values were 1.33 ± 0.18 eV for tetragonal Cu_2SnS_3, and 1.15 ± 0.18 eV for monoclinic Cu_2SnS_3. These values are consistent with those obtained by UV-Vis spectroscopy.

Acknowledgements

R. Garza-Hernández expresses her gratefulness to CONACYT for the scholarship grant N° 401864. The authors acknowledge Tim Joyce from Nanoinvestigation Centre at Liverpool (NiCaL) for the facilities provided to carry out the measurements of EDX-SEM, also Laura Cabo-Fernandez and Jonathan Major from the University of Liverpool for their support in the Raman and UV-Vis measurements, respectively. HJE and JTG thank EPSRC for studentship support.